Spectroscopic, Magnetic, and Optical Characterization of Nanocomposite Films of Polyvinylpyrrolidone Doped with Cerium Disulphate

M. A. F. Basha

Physics Department, Faculty of Science, Cairo University, Giza, Egypt

Received 25 November 2010; accepted 7 February 2011
DOI 10.1002/app.34295
Published online 13 June 2011 in Wiley Online Library (wileyonlinelibrary.com).

ABSTRACT: New nanocomposite hybrid films of a well dispersed cerium disulphate $Ce(SO_4)_2$ nanoparticles into the polyvinylpyrrolidone (PVP) matrix were prepared by a casting technique. The nanostructural nature and complex formation were investigated using the transmission electron microscopy (TEM), the nuclear magnetic resonance (NMR), and the Infrared (IR) spectroscopy. The magnetic measurements at room temperature, using a vibrating sample magnetometer (VSM), and the obtained magnetic parameters revealed that the investigated nanocomposites belong to a category of magnetically soft materials that find widespread applications in contemporary fine technologies. Optical absorption spectra were measured in the ultraviolet (UV)–visible region and the fundamental absorption edge E_a, the energy gap E_g and width of the tail of localized states E_e were evaluated and discussed in terms of the solid band theory. The monotonic increase of these optical parameters with the dopant concentration may be attributed to probable segregation effects occurring in the amorphous host matrix.
 J Appl Polym Sci 122: 2121–2129, 2011

Key words: polyvinylpyrrolidone; cerium disulphate; magnetic nano-composites; optical absorption; VSM; IR, NMR spectroscopy

INTRODUCTION

The interest in novel structures and properties of polymeric blends and composites still motivates in recent years extensive studies, as does the increasing importance in practical applications of new polymeric products having widely ranging physical and physicochemical properties without parallel in pure homopolymers.[1–6]

In this respect, the polymeric composite systems containing rare-earth metal salts belong to a rapidly advancing branch in polymer science and technology, particularly in the synthesis of polymeric nanostructures.[7–12] The resulting nanostructures, in particular, exhibit exclusive functionalities originated from both polymers and inorganic additives, and thus they have received remarkable attention because of their potentially promising applications in the fabrication of plastic lasing materials and electrochemical devices.[7,13,14] Magnetic polymeric nanocomposites, from another side, are of great interest for utilization in high speed and high capacity optical and magnetic information storing media.[15,16] Recently, there has been considerable interest in magneto-optical devices which combine magnetic and optical phenomena.[17] However, the techniques and methods used to synthesize, fabricate and characterize polymer inorganic nanoparticles (NPs) composite materials have been awaited to be developed.

The afore-mentioned arguments stand up for the author's choice of some rare earth metal-doped polymers to be a subject of systematic comparative studies, to find similarities and differences in polymer properties, keeping in mind the importance of the investigations of various additives in the synthesis and characterization of the resulting composites.[10–12] He has recently investigated some structural, magnetic and optical properties of PVP thin films doped with the rare-earth halides $GdCl_3$ or $HoCl_3$.[12]

In the present follow-up study, the rare earth metal salt cerium (IV) sulfate has been selected as an additive to the polymer PVP for a similar purpose. A detailed literature survey indicated that there is nothing available, to the author's knowledge, on the physical properties of the nanocomposite system PVP-$Ce(SO_4)_2$.

Tetrahydrated cerium sulfate $Ce(SO_4)_2.4H_2O$, from one side, is a crystalline compound of little solubility in water, used as highly active oxidant in the synthesis of polymers. Its complete structure determination is still ambiguous and investigations of its polymorphic forms revealed obvious disagreement among different references.[18,19]

The water-soluble and physiologically inert polyvinylpyrrolidone (PVP), from the other side, is a

Correspondence to: M. A. F. Basha (mafbasha@gmail.com).

highly amorphous polymer, characterized by its unusual colloidal and complexing properties, and it has been extensively used as a film-forming or coating material with good optical quality and mechanical strength. It finds widespread applications in the synthesis of nanostructures. It behaves adhesively in many solid substrates. Besides, the pyrrolidone rings in PVP contain a proton accepting carbonyl moiety and prefer to complex with many inorganic salts, resulting in fine dispersion and surface passivation of them.[3,8]

The present article describes the synthesis of new PVP-$(CeSO_4)_2$ nanocomposite thin films by a casting technique with the purpose of investigating a probable complex formation. Also, systematic studies were attempted on the structural, magnetic and optical properties of the prepared samples to better characterize them in terms of the relevant theories, and to determine some of their physical parameters.

EXPERIMENTAL

PVP with FW = 40,000 was supplied by GFS chemicals, Powell, OH. The transition metal salt cerium disulphate, with empirical formula $Ce(SO_4)_2.4H_2O$, FW 404.30, and purity 99.9%, was supplied by Strem Chemicals, Newburyport, MA.

The solution method was used to obtain film samples. A known amount of PVP granules was dissolved in doubly distilled water to prepare a clear solution. Also, known amount of $Ce(SO_4)_2.4H_2O$ salt was dissolved in small amount of distilled water containing few drops of 0.1*M* H_2SO_4 at room temperature. Solutions of $Ce(SO_4)_2.4H_2O$ and PVP were mixed together with different weight percentages, 2, 5, 10, and 15 wt % $Ce(SO_4)_2$, using a magnetic stirrer, at 50°C on a water bath for several hours to obtain complete dissolution. Higher dopant concentrations were difficult to obtain because of its limited solubility in water (36 g L^{-1}, at 50°C). Thin films of appropriate thickness ($\sim$ 80 μm) were cast onto glass Petri dishes, and then dried in air at room temperature for about 7 days until the solvent was completely evaporated.

Morphological investigations were performed using a transmission electron microscope of the type Jeol JEM-1230 (Jeol, Tokyo, Japan) at a working voltage of 100 keV. Images were recorded under an axial illumination at approximate nanoscale focus. The diameter of the objective aperture used was 1 μm. The particle size distribution was determined for the particles of diameters up to 100 nm by measuring the maximum diameter of more than 300 particles along a fixed direction on the micrographs.

^1H NMR and ^{13}C NMR spectra were recorded at room temperature (in DMSO + D_2O) using Varian Gemini 200 MHz NMR spectrometer, Santa Clara, CA.

A vibrating sample magnetometer of the type VSM-9600-1 (LDI Electronics, Troy, MI) was used to determine hysteresis loops for prepared samples at room temperature and applied magnetic fields up to 8 kOe.

The IR spectral analysis was performed using a PYE Unicam spectrophotometer (Pye Unicam, Cambridge, UK) over the wavenumber range of 500–4000 cm^{-1}. The UV–visible absorption spectra of the samples under investigation were carried out employing a Berkin-Elmer 4-B spectrophotometer (Perkin–Elmer, Waltham, MA) in the wavelength range 200–800 nm.

RESULTS AND DISCUSSION

Transmission electron microscopy (TEM)

Figure 1(A,B) shows a typical TEM overview of $Ce(SO_4)_2$ nanoparticles (NPs)in the samples [A] PVP + 5 wt % $Ce(SO_4)_2$ and [B] PVP + 15 wt % $Ce(SO_4)_2$, respectively. It can be seen that the additive salt is properly dispersed in the PVP matrix and the samples under investigation are nanostructured materials. The images also show that the shape of the particles in Figure 1(B) appears spherical, and the distance between the particles appears relatively shorter than that in Figure 1(A).

Figure 1(C,D) shows the histograms of the particles size distribution in the PVP + 5 wt % $Ce(SO_4)_2$ and PVP + 15 wt % $Ce(SO_4)_2$ samples, respectively. Statistical results revealed that the values of the average particle size for samples [A] and [B] are 43.75 and 68.14 nm, respectively. It can be observed that more agglomerated particles, at the expense of separated ones, are present in the sample containing relatively higher concentration of the dopant.

Mainly, the nanoparticles containing cerium ions experience a resultant permanent magnetic moment proportional to their volume.[20] Hence the particles are permanently magnetized and possess a tendency to agglomerate. The agglomeration can also be partly attributed to some extent to electrostatic or Van der Waals' forces between particles.

IR spectra

Figure 2 shows the infrared transmittance spectra and the assignments of the most evident absorption bands of pure PVP and $Ce(SO_4)_2.4H_2O$ samples, together with their composites in the wavenumber range 500–4000 cm^{-1}.

$Ce(SO_4)_2.4H_2O$ infrared spectrum (a) contains a characteristic intense peak at 1628 cm^{-1}, in addition to a broad band at about 3320 cm^{-1} related to the

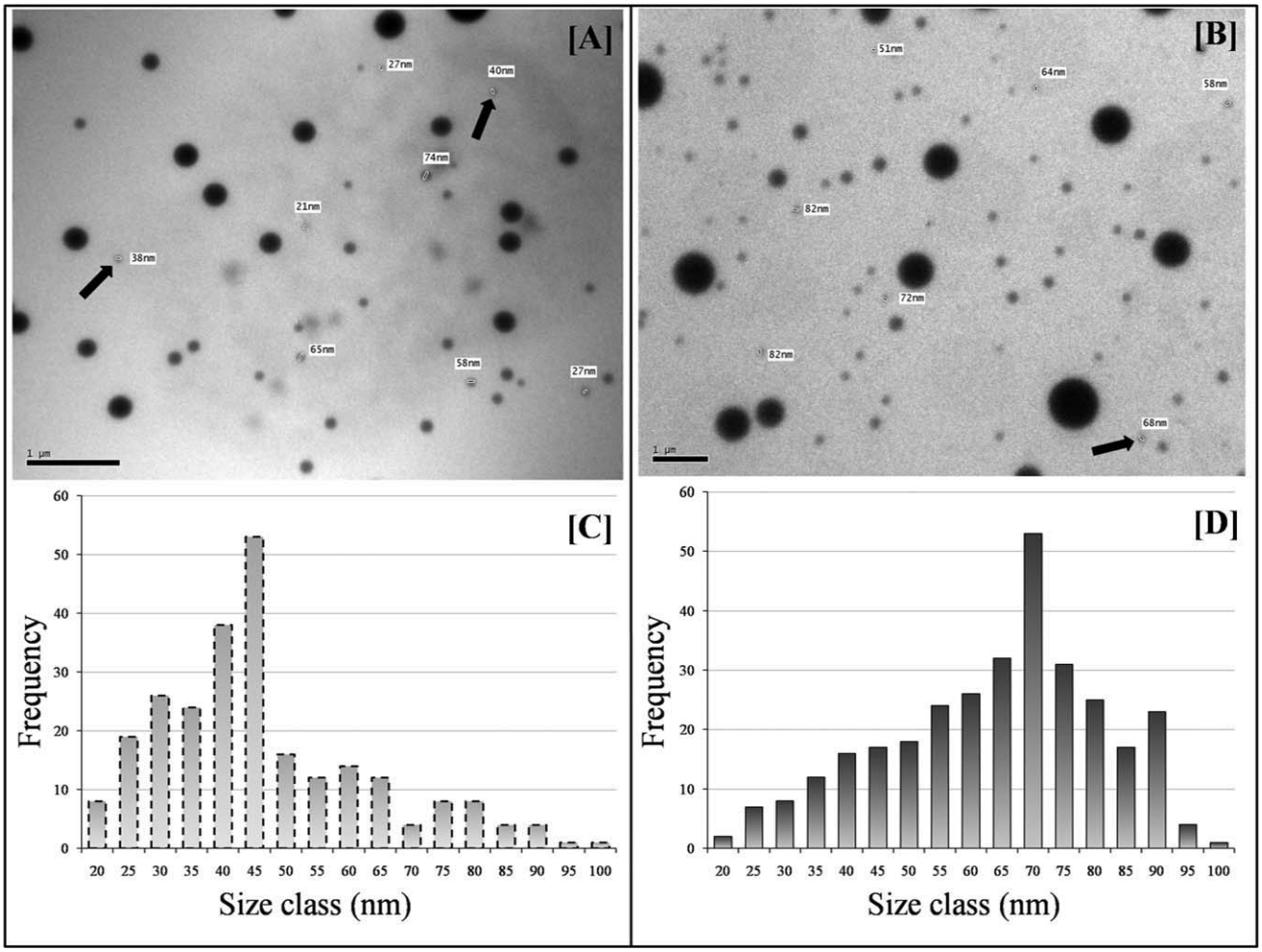

Figure 1 TEM images of the samples: (A) PVP + 5 wt % $Ce(SO_4)_2$ and (B) PVP + 15 wt % $Ce(SO_4)_2$. The corresponding histograms (C) and (D) present the particle size distribution. The arrow indicates examples of the average particles size.

δ(HOH) bending and $\upsilon_{as,s}$(HOH) stretching vibrations of the coordinated water molecules. Other bands, probably due to sulfate groups, can be observed at 598 cm^{-1} (ν_4) and 1115 cm^{-1} (ν_3), in addition to a small band at 673 cm^{-1} (ν_1) corresponding to metal-oxygen and metal-hydroxide bonding.[21,22]

In contrast, the PVP infrared spectrum (b) contains the main peaks corresponding to the majority of vibrational modes, in spite of the symmetry decrease entailed by the existence of the heteroatom and a carbonyl group in the pyrrolidone ring. Table I indicates that the empirical assignments of the most evident absorption bands for pure PVP thin film investigated in the present work are consistent with those previously reported in the literature.[12,23] The relatively broad υ(OH) stretching band centered at about 3450 cm^{-1} indicates the presence of stretching vibration associated with free and numerous hydroxyl groups (OH^-), in addition to hydrogen-bonded (H—O—H) due to residual water because of not using vacuum drying for the investigated samples.

The observed characteristic band of PVP at 1675 cm^{-1} is due to the carbonyl (C=0) stretching, which is very sensitive to hydrogen bond formation with water molecules. Some authors reported that the υ(C=0) shifts from 1680 to 1652 cm^{-1} as the concentration of absorbed water is increased.[12,24]

In addition, the distinctive doublet appearing at 2362 and 2342 cm^{-1}, along with a small broad peak at 2134 cm^{-1}, are clearly evident in the obtained spectrum of pure PVP.

Figure 2 shows also the IR spectra c, d, e, and f which characterize the PVP thin films doped with 2, 5, 10, and 15 wt % ceric sulfate, respectively. At the first glance, one can find that the main typical bands of both the polymer and dopant are greatly affected in shape, intensity and position with their composition ratio in the composites under investigation.

Careful examination of the IR spectra of these composites showed that the addition of $Ce(SO_4)_2$ to PVP makes the band at 3450 cm^{-1} more intense with a slight shift ($\sim$ 24 cm^{-1}) toward lower wavelengths, and entails the split of the small overlapped

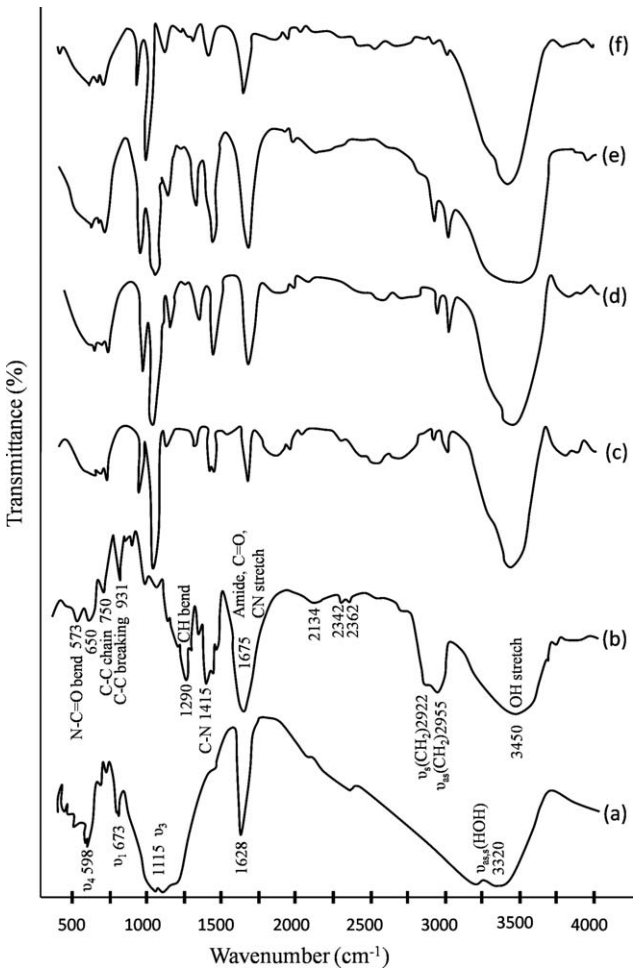

Figure 2 IR spectra of (a) $Ce(SO_4)_2.4H_2O$, (b) PVP, (c) 2, (d) 5 and (e) 10 and (f) 15 wt % $Ce(SO_4)_2$-doped PVP.

bands at 2955 and 2922 cm^{-1} into two gradually distinguished sharp bands at 2998 and 2914 cm^{-1} for all dopant concentrations, except that of 15 wt % $Ce(SO_4)_2$ in which these sharp bands seemed to be nearly diminishing (spectrum f).

Besides, the two bands assigned to C—N and CH bending modes at 1494 and 1373 cm^{-1}, respectively, became well sharply defined with varying intensity and remarkable shift to 1429 and 1316 cm^{-1}, respectively. Also, very intense sharp band at 1061 cm^{-1} between other two relatively small sharp bands at 1115 and 980 cm^{-1} have been developed in the spectra of all composites, probably due to the sulfate group incorporated in the polymeric complex.[21]

On the other hand, the position of the characteristic band at 1675 cm^{-1} exhibited an irregular decrease (about 17 cm^{-1}) with the increase of dopant concentration. It is worth noting that the presence of some weak sidebands and shoulders shown in the spectra of the investigated samples arises because of vibronic coupling.

All those observed peak shifts and changes in shapes and intensities provide strong support to the formation of complexation between PVP backbone and nanoparticles (NPs) of cerium disulphate. The pyrrolidone groups of PVP prefer to complex with cerium disulphate NPs, resulting a fine dispersion and surface passivation of them.[8]

NMR characterization

Figure 3(a) demonstrates the ^1H NMR analysis of pure PVP dissolved in DMSO+D_2O. It revealed the presence of two signals appeared at 1.9 and 2.07 ppm, corresponding to the methylene protons H-7 and H-4. Furthermore, signals at 3.15, 3.54, and 3.77 ppm are related to H-3, H-5, and H-6, respectively.[3,4,25]

On the other hand, ^1H NMR spectrum of the PVP/$Ce(SO_4)_2$ composite (90 : 10 w/w) dissolved in DMSO + D_2O showed that a probable partial complexation may be occurred due to the presence of peak shape variation and downfield shift of the signal at 3.77 ppm to appear at 4.57 ppm, and the appearance of two new signals at 5.02 and 5.32 ppm which are still of unspecified assignments, Figure 3(b).

Figure 4(a) shows a characteristic signal of ^{13}C NMR of PVP at 174.41 ppm related to cyclic amide carbonyl carbons (C-2) of the pyrrolidone ring. Furthermore, methylene carbons signals at 18.16 and 30.13 ppm are attributed to C-7 and C-4, respectively. Besides, methylene carbons of the pyrrolidone ring at 41.74 and 43.67 ppm corresponding to C-3 and C-5, respectively, are present. Finally, a methine carbon signal at 44.75 ppm is related to C-6.[3,4,25]

Figure 4(b) depicts the ^{13}C NMR spectrum of the PVP/$Ce(SO_4)_2$ composite (90 : 10 w/w) dissolved in

TABLE I
The Assignments of IR Absorption Bands for Pure PVP Thin Film

Frequency (cm^{-1})	Assignment
3741	broad OH stretch
3450	
2955	asym CH_2 stretch, ring
2922	sym CH_2 stretch, chain
1675	amide, C=O, C—N stretch
1494	C—N
1462	CH_2 sissor
1427	
1373	CH bend
1286	CH_2 wag, C—N stretch
1228	CH_2 twist
1170	
1019	C—C, CH_2 rock
931	C—C, ring breathing
845	C—C, ring
750	C—C, chain
650	N—C=O bend, ring def.
573	

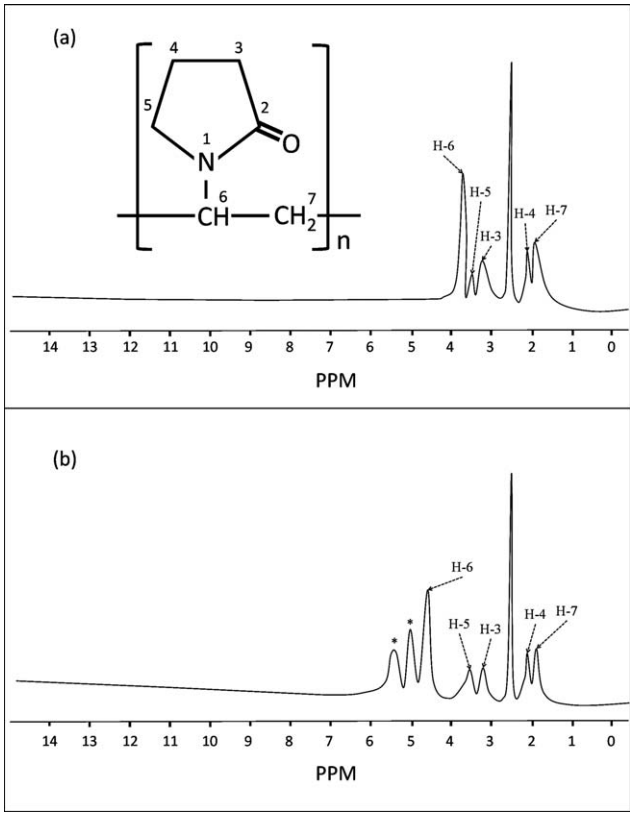

Figure 3 ^{1}H NMR spectra of (A) PVP and (B) the composite PVP + 10 wt % $Ce(SO_4)_2.4H_2O$ dissolved in DMSO+ D_2O at room temperature. The Mark (*) in (B) indicates new signals. Inset of (A): Chemical structure of PVP.

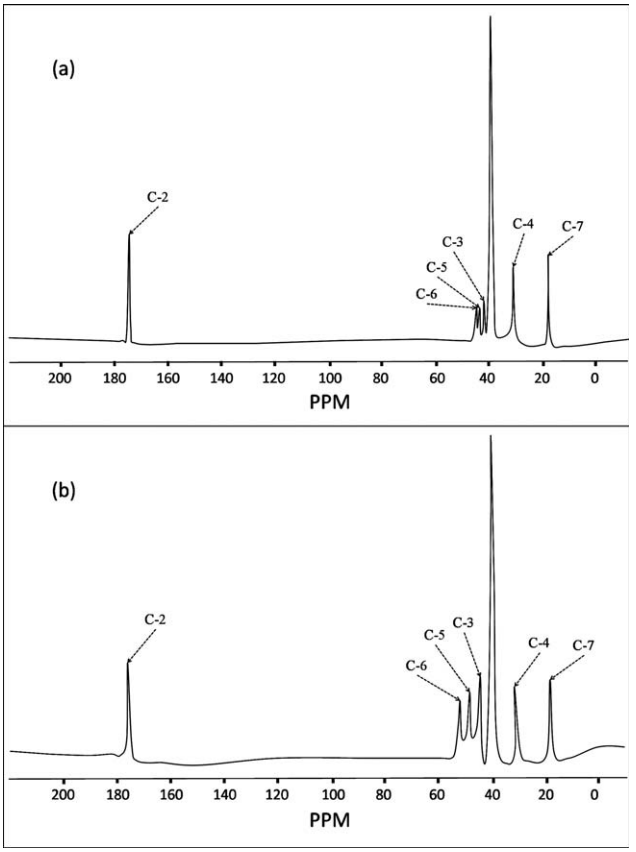

Figure 4 ^{13}C NMR spectra of (A) PVP and (B) the composite of PVP + 10 wt % $Ce(SO_4)_2.4H_2O$ dissolved in DMSO at room temperature.

DMSO. The observed downfield shift of the signal related to methylene carbon C-5 to appear at 47.29 ppm and that related to the methine carbon C-6 to appear at 52.30 ppm may be also due to partial complex formation depending on dopant concentration.

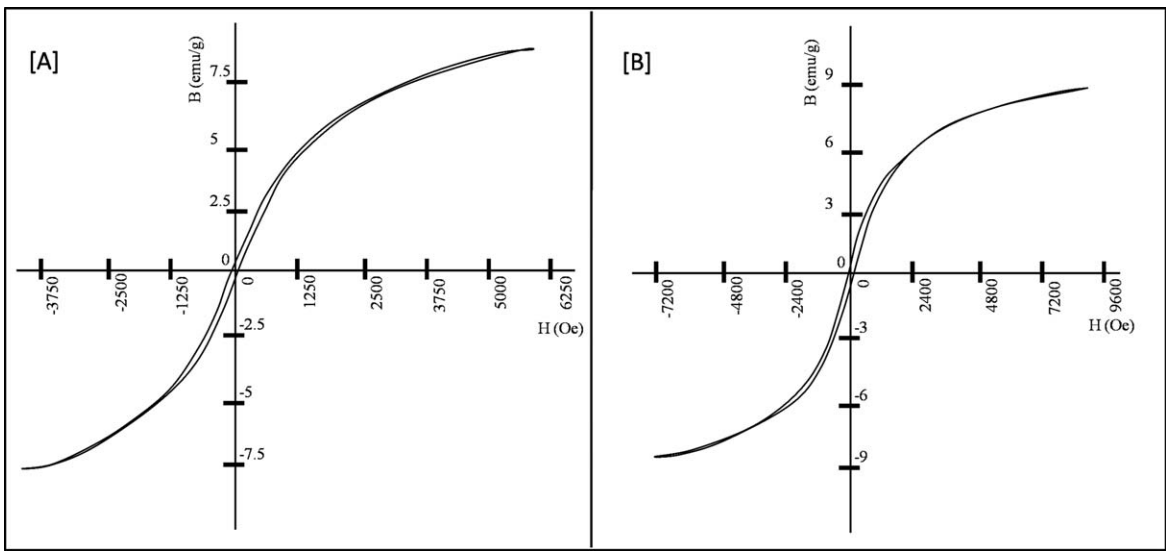

Figure 5 Representative *B–H* loops for (A) the composite film PVP + 5 wt % $Ce(SO_4)_2$ and (B) the composite film PVP + 10 wt % $Ce(SO_4)_2$ at room temperature.

TABLE II
The *B–H* Curve Parameters Characterizing the Investigated Films of the Magnetic Nanocomposites of the PVP-$Ce(SO_4)_2$ Systems

Sample	B_s (e.m.u.g^{-1})	B_r (e.m.u.g^{-1})	$\frac{B_r}{B_s}(SQR)$	$H_c(O_e)$	μ_{max}
PVP + 2 wt % $Ce(SO_4)_2$	8.14	0.35	0.043	34.20	5.084
PVP + 5 wt % $Ce(SO_4)_2$	8.39	0.31	0.036	42.75	6.300
PVP + 10 wt % $Ce(SO_4)_2$	8.71	0.57	0.065	35.56	5.102
PVP + 15 wt % $Ce(SO_4)_2$	8.37	0.53	0.063	37.04	5.573

Magnetic properties

In previous work,[12] the author has made magnetic studies on nanostructured thin films of PVP-$GdCl_3$ and PVP-$HoCl_3$ composite systems by measuring their magnetization versus the magnetic field at room temperature and finding their magnetic characteristics. In the present follow-up study, the hysteresis loops of the investigated PVP-$Ce(SO_4)_2$ magnetic nanocomposites were measured using a vibrating sample magnetometer (VSM) at room temperature and applied fields up to 10 kOe to determine magnetic parameters such as the saturation magnetic flux density (B_s), remanent magnetic flux density (B_r), squareness ratio, SQR (B_r/B_s) and coercive field (H_c). The maximum permeability μ_{max} was also determined from the *B–H* relations. Representative *B–H* loops are given in Figure 5 and the obtained results are summarized in Table II.

It is clear from Figure 5 and Table II that the values of magnetic *B–H* parameters are composition dependent and the composite film PVP + 5 wt % $Ce(SO_4)_2$ shows slightly better magnetic characteristics than the other samples.

As a matter of experimentation, the appearance of hysteresis loops, although with relatively small values of B_s, B_r, SQR, and H_c, along with permeability values μ_{max} relatively higher than 1, may allow one to confirm a magnetically soft behavior at room temperature for the samples under investigation.[26–29] The uniform distribution of permanently magnetized rare earth nanoparticles in the PVP matrix, as illustrated by TEM images (Fig. 1), is critical in developing the experimentally established magnetic behavior for the investigated nanocomposites.

Optical properties

The UV–vis absorption spectrum is a powerful tool for understanding the band structure and electronic properties of pure and filled polymers. It gives valuable information about the electronic transitions from the valence band to the conduction band. The transition is direct when the wave vector for the electron remains unchanged, but in the case of indirect transition, interaction with a lattice vibration (phonon) occurs.[30]

Figure 6 shows the absorption spectra of pure PVP (spectrum a), Pure $Ce(SO_4)_2$ (spectrum b), together with the spectra c, d, e and f for the composites containing 2, 5, 10, and 15 wt % $Ce(SO_4)_2$, respectively, in the UV–visible range 200–700 nm.

The spectrum (a) of pure PVP exhibits a well-defined absorption band at 249 nm, along with a small shoulder at 280 nm, and ill-defined band at 380 nm. The spectrum (b) of the pure cerium compound shows a gradual increase towards lower wavelength, reaching a broad shoulder-like absorption peak at $\sim$ 290 nm, followed by remarkable identical absorption band at about 235 nm in the UV region.

The addition of $Ce(SO_4)_2$ to PVP has led to the disappearance of the ill-band of PVP at about 380 nm, and entailed changes in shape, intensity and position of the shoulder observed at 280 nm and the

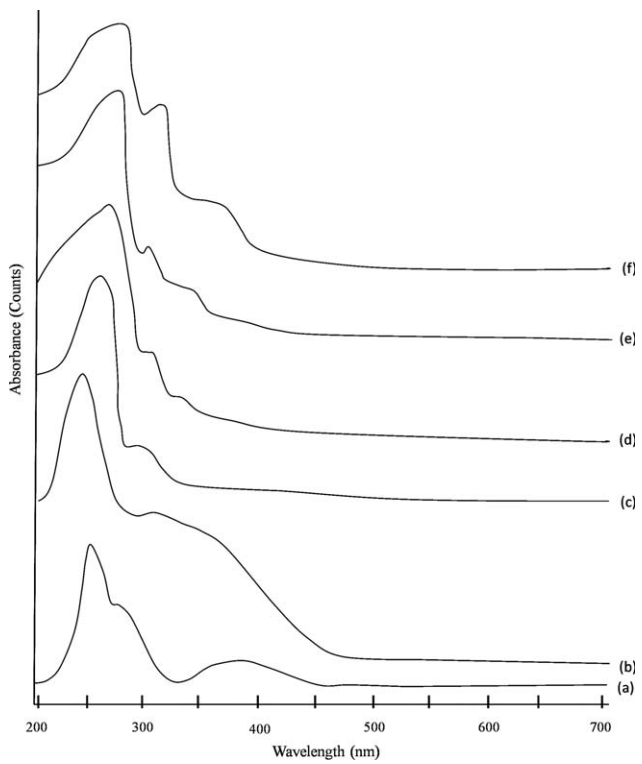

Figure 6 UV–visible spectra of (a) pure PVP, (b) pure $Ce(SO_4)_2.4H_2O$, (c) 2, (d) 5, (e) 10 and (f) 15 wt % $Ce(SO_4)_2.4H_2O$-doped PVP.

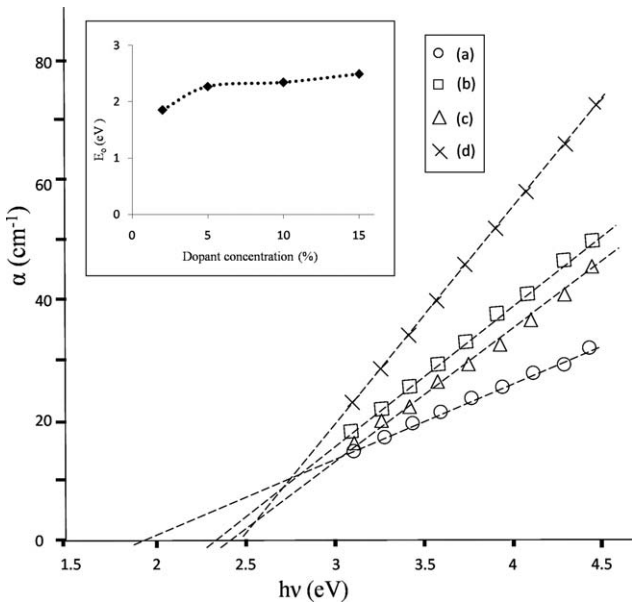

Figure 7 Plots of α versus $h\upsilon$ for (a) 2, (b) 5, (c) 10, and (d) 15 wt % $Ce(SO_4)_2.4H_2O$ doped PVP. Inset: Variation of absorption edge E_o (eV) with dopant concentration.

peak appeared at 249 nm, with slight gradual shift towards higher wavelengths.

The absorption coefficient α is directly determined from the spectra by the relation:

$$\alpha(\nu) = \frac{1}{d}\ln\left(\frac{1}{T}\right) = \frac{2.303}{d}A(\nu)$$

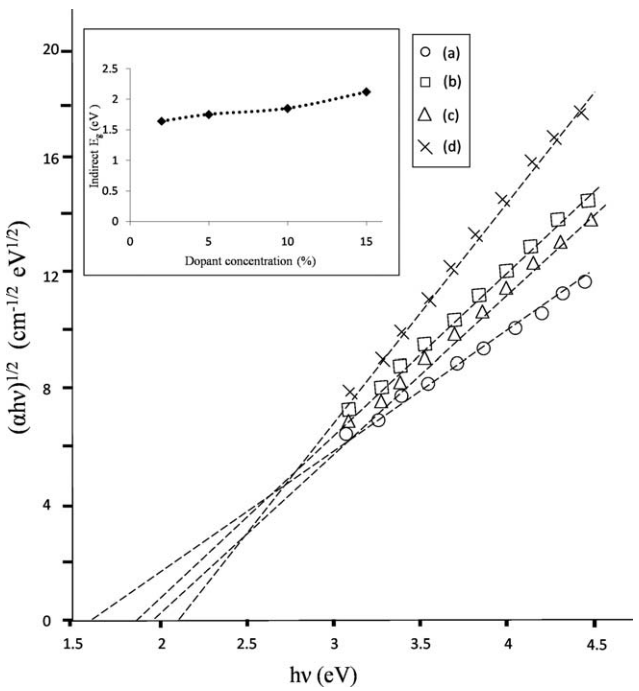

Figure 8 Plots of $(\alpha h\upsilon)^{1/2}$ versus $h\upsilon$ for (a) 2, (b) 5, (c) 10, and (d) 15 wt % $Ce(SO_4)_2$. $4H_2O$-doped PVP. Inset: Variation of indirect optical band gap E_i (eV) with dopant concentration.

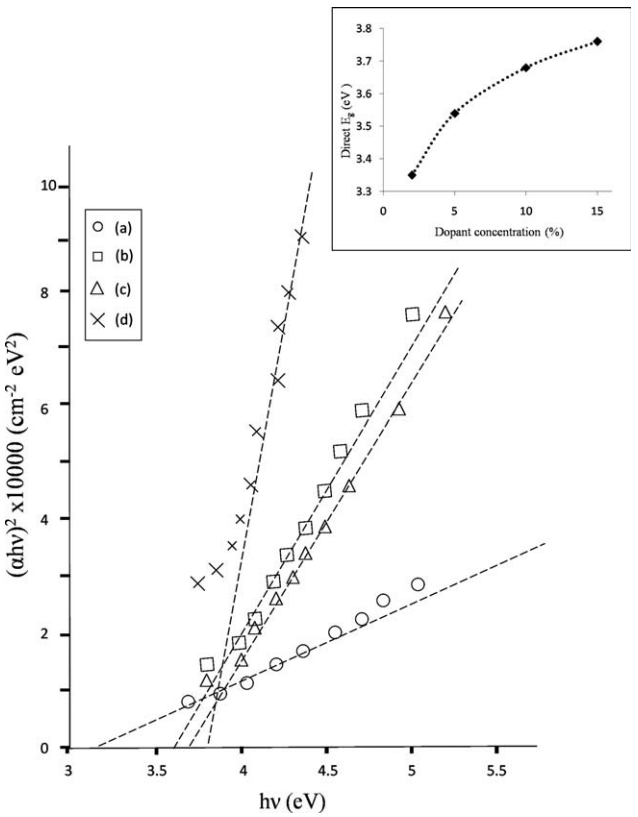

Figure 9 Plots of $(\alpha h\upsilon)^2$ versus $h\upsilon$ for (a) 2, (b) 5, (c) 10, and (d) 15 wt % $Ce(SO_4)_2$. $4H_2O$-doped PVP. Inset: Variation of direct optical band gap E_d (eV) with dopant concentration.

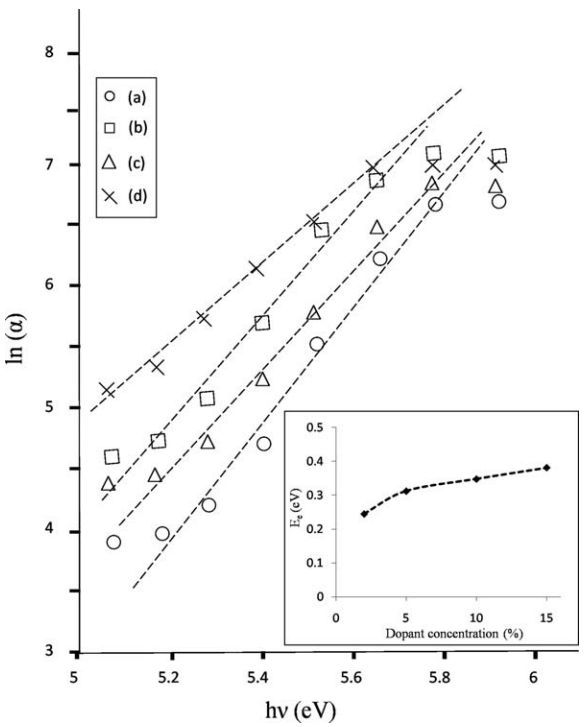

Figure 10 Plots of *ln* α versus $h\upsilon$ for (a) 2, (b) 5, (c) 10, and (d) 15 wt % $Ce(SO_4)_2.4H_2O$-doped PVP. Inset: Variation of Urbach tail Ee with dopant concentration.

TABLE III
Absorption Edge Position, Direct and Indirect Optical Band Gap, and Urbach Tail for PVP-$Ce(SO_4)_2$ Nanocomposite Films

Sample	Absorption edge E_o (eV)	Band gap E_g (eV)		Urbach tail E_e (eV)
		Indirect E_i	Direct E_d	
PVP	2.65	2.42	2.80	0.28
PVP + 2 wt % $Ce(SO_4)_2$	1.85	1.64	3.35	0.25
PVP + 5 wt % $Ce(SO_4)_2$	2.27	1.75	3.54	0.31
PVP + 10 wt % $Ce(SO_4)_2$	2.34	1.85	3.63	0.35
PVP + 15 wt % $Ce(SO_4)_2$	2.49	2.12	3.76	0.38

where T is the transmittance, A is the absorbance and d is the thickness of the film.

Making use of the solid band theory,[5,31–33] the variation of α, $(\alpha h\upsilon)^{1/2}$, $(\alpha h\upsilon)^2$ and $\ln(\alpha)$ with incident photonenergy $h\upsilon$ enables one to determine the absorption edge E_o, the indirect transition energy E_i, the allowed direct transition energy E_d and the Urbach tail E_e, respectively, for the investigated samples, following the procedures described in previous works.[12,31] Figures 7–10 depict the corresponding relations, and Table III summarizes the calculated energies characterizing the investigated composites. The insets show a general trend of monotonic increase of the calculated physical parameters with the increase of dopant concentration. This behavior may be partly attributed to probable segregation effects occurring in the polymeric amorphous matrix.[34]

The variation of the calculated values of the optical energy gaps may reflect the role of $Ce(SO_4)_2$ additives in modifying the solid band structure of the PVP matrix due to the existence of various defect levels.[30] The density of localized states was found to be proportional to the concentration of these defects[35] and consequently, to the concentration of the $Ce(SO_4)_2$ content. The monotonic increase in the optical band gap with increasing dopant concentration also indicates the increase in the grain size and the reduction in the disorder due to the fact that more spherically agglomerated particles are present in the sample containing relatively higher concentration of the dopant,[36–38] as previously illustrated by TEM images, Figure 1.

These optical changes provide further evidence for a probable complex formation in the composites under investigation, showing good conformity with the information obtained from the IR spectroscopy and magnetic measurements in the previous sections.

CONCLUSIONS

i. A casting technique was used to prepare new hybrid thin films of PVP doped with cerium (IV) sulfate nanoparticles (NPs).
ii. The images of TEM confirmed the nanostructural nature of the investigated composites and showed that agglomerated particles, as well as separated ones, are clearly present in the PVP sample containing 15 wt % $Ce(SO_4)_2$.
iii. The changes in the shape, intensity and position of the characteristic bands of PVP in the IR spectra allow suggesting a complex formation in the investigated composites.
iv. The downfield shifts and their assignments for various carbons in the ^1H NMR and ^{13}C NMR spectra provide further tending support to the formation of PVP-$Ce(SO_4)_2$ complex.
v. The hysteresis loops obtained using a VSM and the determined magnetic parameters revealed that the investigated nanocomposites possess magnetically soft behavior under the conditions of experiment. A permeability value of 6.3 for the composite PVP + 5 wt % $Ce(SO_4)_2$ is the highest among all of the samples.
vi. The UV–visible spectra characterizing the investigated samples were discussed in terms of the solid band theory and the calculated optical parameters were found to increase monotonically with the gradual increase of dopant concentration. This result indicates the effective role of the $Ce(SO_4)_2$ additives in modifying the band structure in the polymer matrix.

References

1. Sheldon, R. P. Composite Polymeric Materials, Applied Science; Elsevier Science: London, 1982.
2. Nishio, Y.; Haratani, T.; Takahashi, T. J Polym Sci B Polym Phys 1990, 28, 355.
3. Kumar, V.; Yang, T.; Yang, Y. Int J Pharm 1999, 188, 221.
4. Jin, S.; Liu, M.; Chen, S.; Gao, C. Eur Polym Mater 2008, 44, 2162.
5. Sharma, A. K.; Ramu, C. H. J Mater Sci Lett 1991, 10, 1217.
6. Abd El-kader, F. H.; Gafar, S. A.; Basha, A. F.; Banana, S. J.; Basha, M. A. F. J Appl Polym Sci 2010, 118, 413.
7. Twomey, C. J.; Chen, S. H. J Polym Sci B Polym Phys 1991, 29, 859.

8. Feng, W.; Tao, H.; Liu, Y. J Mater Sci Technol 2006, 22, 230.
9. Giuffrida, S.; Condorelli, G. G.; Costanzo, L. L.; Ventimiglia, G.; DiMauro, A; Fragala, I. L. J Photochem Photobiol A Chem 2008, 195, 215.
10. Abdel Kader, F. H.; Osman, W. H.; Ragab, H. S.; Shehap, A. M.; Rizk, M. S.; Basha, M. A. F. J Polym Mater 2004, 21, 49.
11. Abdel Kader, F. H.; Osman, W. H.; Mahmoud, K. H.; Basha, M. A. F. Phys B 2008, 403, 3473.
12. Basha, M. A. F. Polym J 2010, 42, 728.
13. Oczko, G.; Macalik, L. Polyhedron 2010, 29, 1231.
14. Koechner, W. Solid-State Laser Engineering, 2nd ed.; Springer-Verlag: New York, 1988.
15. Ao, B.; Kummerl, L.; Haarer, D. Adv Mater 1995, 7, 496.
16. Mallinson, I. C. The Foundation of Magnetic Recording; Academic Press: Berkeley, 1987; Chapter 3.
17. Kang, Y. S.; Lee, D. K.; Stroeve, P. Thin Solid Films 1998, 327/392, 541.
18. Casari, B. M.; Langer V. J Solid State Chem 2007, 180, 1616.
19. Lindgren, O. Acta Chem Scand A 1977, 31, 453.
20. Gabal, M. A. J Magn Magn Mater 2009, 321, 3144.
21. Valeri, P. T.; Irina, V. C.; Valeri, A. S. Handbook of Infrared Spectroscopy of Ultrathin Films; Wiley: New York, 2003; Chapter 3, p 140.
22. Gadsden, J. A. Infrared Spectra of Minerals and Related Inorganic Compounds; Butterworth Group: USA, 1975; Part II, p 11.
23. Borodko, Y.; Habas, S. E.; Koebel, M.; Yang, P.; Frei, H.; Somorjai, G. A. J Phys Chem B 2006, 110, 23052.
24. Taylor, L. S.; Langkilde, F. W.; Zografi, G. J Pharm Sci 2001, 90, 888.
25. Aldeyeye, C. M.; Barabas, E. Anal Profiles Drug Substances Excipients 1993, 22, 555.
26. Parker, R. J. Adv in Permanent Magnetism; Wiley: New York, 1990.
27. Roy, P. K.; Bera, J. J Magn Magn Mater 2009, 321, 247.
28. Campbell, P. Permanent Magnet Materials and their Application; Cambridge University Press: UK, 1994.
29. Andriessen, F.; Torpstra, M., Eds. Rare Earth Metals Based Permanent Magnets; Elsevier Applied Science: UK, 1989.
30. Zidan, H. M. Abu-Elnader, M. Phys B 2005, 355, 308.
31. Al-Ani, S. K. J.; Hogarth, C. A.; El-Malawany R. A. J Mater Sci 1985, 20, 661.
32. Chopra, N.; Mansingh, A.; Chadha, G. K. J Non-Cryst Solids 1990, 126, 194.
33. Kuku, T. A. J Mater Sci 1998, 33, 3193.
34. Devi, C. U.; Sharma, A. K.; Rao, V. V. R. N. Mater Lett 2002, 56, 167.
35. Mott, N. F. Philos Mag 1970, 22, 7.
36. Urbach, F. Phys Rev 1953, 92, 1324.
37. Ilyas, M.; Zulfequar M.; Husain M. J Mod Opt 2000, 47, 663.
38. Nang T. T.; Okuda, M.; Matsushita, T.; Yokota, S.; Suzuki, A. Jpn J App Phys 1976, 14, 849.